IEEE Access
Multidisciplinary ⋮ Rapid Review ⋮ Open Access Journal

Received August 24, 2021, accepted September 8, 2021, date of publication September 10, 2021,
date of current version September 21, 2021.

Digital Object Identifier 10.1109/ACCESS.2021.3111956

Ring-Embedded Micro-Power mm-Sized Optical Sensor for Accurate Heart Beat Monitoring

ASSIM BOUKHAYMA, ANTHONY BARISON, SERJ HADDAD, AND ANTONINO CAIZZONE, (Member, IEEE)
Senbiosys SA, 2000 Neuchâtel, Switzerland

Corresponding author: Assim Boukhayma (assim.boukhayma@senbiosys.com)

This work involved human subjects or animals in its research. The authors confirm that all human/animal subject research procedures and protocols are exempt from review board approval.

ABSTRACT This paper presents a wearable optical health monitoring device embedding a monolithic sensor chip with newly designed pixels, and an optical module optimized for photoplethysmography (PPG). The monolithic optical sensor at the heart of this device implements an array of novel pixels designed specifically for PPG and featuring a quantum efficiency (QE) as high as 85%. The sensor readout chain, as well as the logic circuits, implements low power design techniques leading to only 60 μA current consumption at 122 Hz operation frequency, including digital communication. Thanks to the high QE and optical module optimization, medical grade PPG recordings are enabled with less than 10 μA emitter current. The optical sensor is embedded in an ergonomic ring device together with system electronics in order to enable in-field test of beat detection accuracy on 7 subjects. The ring device detects correctly 97.87% of the beats on a total of 72.21 hours of recording. The inter-beat interval (IBI) estimation from these recordings features a mean absolute error (MAE) as low as 8.10 ms. This performance is achieved with less than 70 μA current consumption at the level of the PPG module.

INDEX TERMS CMOS image sensor, heart beat detection, low power integrated circuit, monolithic optical detector, photoplethismography sensor, wearable electronics.

I. INTRODUCTION

Remote health monitoring, based on wearable-integrated sensors, provides these days more and more alternatives to standard healthcare practices. Indeed, the modern society suffers from an increase in cardiovascular-diseases (CVDs) case, resulting from the population ageing and the growing obesity rates. This imposes huge economical implications and, as a matter of fact, is calling out for cost-effective and reliable wearable health monitoring devices.

Heart rate monitoring by the means of optical transduction has revolutionized the smartwatches and fitness band segment and proven the huge implication of those devices to improve people's lifestyle and wellness. The science and sensing scheme behind the optical heart rate monitors is the so called Photoplethysmography (PPG). It has been proven that this technology enables non-invasive monitoring of vital signs well beyond the heart rate, including the blood oxygen saturation, the respiration rate, and the arterial blood pressure [1]. The latter, as a matter of fact, is gaining huge interest these days. Despite the PPG sensors have appeared at first in smartwatches and fitness bands, lately, more and more types of wearables are benefiting from the PPG technology. Among them smartrings are getting popularity, particularly in the sleep monitoring application [2], thanks to the longer lifetime coming from the PPG-centered usage. In addition, the PPG signal quality is biased by the body location of the PPG sensor itself, and, in this regard, the finger is considered as one of the best locations in terms of PPG signal quality [3]. This ultimately results into better vitals' extraction and lower power consumption.

A PPG signal is obtained by shining light from one or more LEDs, at a given wavelength, into a human tissue, e.g. finger, wrist, ear lobes. Wavelengths from visible to near-infrared are used. As shown in Fig. 1, a photodetector (PD) detects the light reflected from the tissue and transforms it into a photogenerated current. The PPG signal, i.e. the photogenerated current, features two different components: a large

The associate editor coordinating the review of this manuscript and approving it for publication was Eyhab Al-Masri.

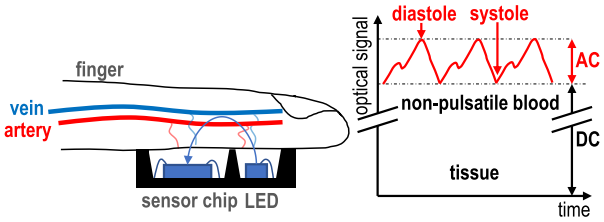

FIGURE 1. Sensor set-up for a PPG measurement and the DC and AC components of a PPG signal.

quasi-DC component corresponding to the light diffusion through tissues and non-pulsatile blood layers, and a small AC part due to the diffusion through the arterial blood. The AC component is typically between 0.2% and 10% of the DC one, depending on several factors including the body location and the body temperature [4]. The ratio between the AC and the DC components is usually referred to as Perfusion-Index (PI). Enhancing the PI for a given power and dynamic range budget is one of the most severe challenges when it comes to engineering a PPG sensor. Indeed, the majority of the medical information is carried by the tiny AC component.

Despite the great interest behind the PPG technology, state-of-the-art (SOA) PPG sensors are still limited by the LEDs power consumption, which usually dominates the PPG sensors' power drill down. Indeed, SOA sensors still leverage a quite standard design paradigm, relying on off-chip photodiodes and standard circuitry, the latter very often based on a transimpedance-amplifier (TIA). This design paradigm often limits the exploitation of these sensors in the remote health monitoring, because of a still fairly large power consumption. Pinned-photodiodes (PPDs) are today the key ingredients of CMOS image sensors (CIS), thanks to their large sensitivity and extremely low-noise operations [5], [6]. It has been shown in [7]–[10] that the excellent performance of a PPD makes it particularly interesting for the PPG application. Indeed, it is possible to reduce the PPG sensor LED average current consumption to a few μA, still achieving very high signal fidelity, the latter being key for any vitals' extraction.

We have recently presented a monolithic micro-power mm-sized PPG sensor integrating an array of newly designed pixels, featuring high quantum efficiency (QE) up to 800 nm. The latter was optimized to operate on an ear worn device (earbud) with a very compact chip and optical module [11], demonstrating medical grade performance for heart beat detection. This paper extends this work and shows that this technology can be exploited in another wearable PPG use case: the smartring. In this regard, a new chip featuring a larger size together with a larger optical module are specifically designed for this ring application. A medical grade heart beat detection with less than 10 μA LED current has been achieved thanks to the efficient coupling of the optical module into an ergonomic and compact ring. As a matter of fact, the different optimization layers enabling this performance, in terms of optical module and wearable system, are also described. This work is organized as follows: Section II

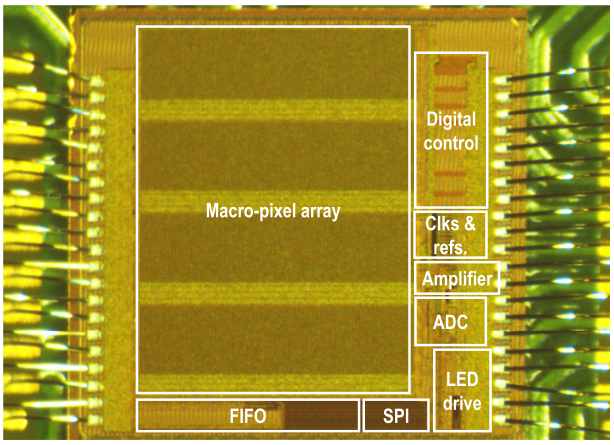

FIGURE 2. Die micrograph showing the 2.5 mm by 2.5 mm sensor main building blocks integrated with pixels array.

briefly overviews the working principle behind the proposed PPD pixels and also introduces the micro-power mm-sized PPG sensor. Section III presents how the micro-power PPG chip is integrated together with the LEDs, module-wise, in order to enhance the PPG performance. Section IV describes the strategy to integrate the PPG module into a smartring in order to ensure ergonomics. The performance measurements of the optical module are shown in Section V. Section VI reports how the smartring data are processed to achieve accurate heart beat monitoring. Section VII highlights the advantages of the proposed PPG monolithic chip and module in the smartrings use case. Finally, Section VIII concludes the paper.

II. A MICRO-POWER mm-SIZED MONOLITHIC PPG SENSOR

The use of a monolithic chip for a ring device reduces the integration constraints. Indeed, it reduces the number of discrete elements that need to be placed on a flexible, or curved, platform. The chip presented in [11] shows a good example of the miniaturization level that can be achieved thanks to the implementation of a monolithic CIS technology. The latter implementation targeted an ear worn device. The PPG signal depends dramatically on the body location. The finger PPG PI is more dependent on ambient temperature drop compared to ear PPG, where the skin is less affected by hypothermia, unlike the limbs. Hence, in contrast to [11], a larger pixel array is needed to collect more signal in the case of a PI drop. Fig. 2 shows a micrograph picture of the monolithic chip designed for finger PPGs. This chip is fabricated in a 180 nm CIS four metal process and features a size of 2.5 mm by 2.5 mm. Similarly to [11], this PPG sensor is a standalone chip embedding its own oscillators, LED drivers with two time division multiplexed channel to operate two LED wavelengths, an integrated array of dedicated pixels, together with a low noise analog readout chain. The latter includes the analog to digital conversion (ADC). For the communication, the chip encompasses a 128 words first-in-first-out (FIFO)

register, and a serial peripheral interface (SPI) communication unit. The photosensitive area embeds an array of pixels exploiting PPD technology to ensure a maximum QE and low noise performance.

The global architecture of the sensor is depicted in Fig. 3, together with a simplified timing diagram. The pixel features a two-tap PPD scheme with deep epitaxial layer, that is detailed in [10]. This offers a good QE, up to the near-infrared (NIR) spectra. The p+np structure of the PPD integrates the electrons generated from the photons impinging on the PPD depleted area. The reset tap (RST) dumps the charge integrated outside the signal integration window. The transfer tap (TX) transfers the charge integrated during the sensing windows. A double sampling scheme is adopted in order to mitigate the ambient light component. All the pixels of a same column share their transferred charge on the same sense node (SN). The SNs are connected to a switchable parallel capacitance that enables the extension of the dynamic range, if needed.

The pixels feature the same well density of $3 \cdot 10^5$ electrons/pixel as in [11]. In this wok, the array is designed to reach a higher DC signal-to-noise-ratio (SNR) of 96 dB to cope with the more challenging PI variation of the finger PPG. Under the assumption of shot noise dominance, the number of photo-electrons required to reach 96 dB is $4 \cdot 10^9$. Therefore, the array encompasses 16384 pixels, split equally between 512 macro-pixels (MP). This array is four times larger than the one presented in [11].

The SNs voltage level is readout thanks to source follower stages (SFs), exploiting native transistors for a maximum voltage swing. Two sample and hold stages are then used for storing the ambient and signal levels and, at the same time, allowing for the averaging of those sampled values by the means of a charge sharing mechanisms over the whole array. This process reduces dramatically the noise contribution of the active SF stages. It also plays the role of buffering the signal to the input of the variable gain amplifier. The latter amplifies the ambient light free signal samples to a low power 14 bit ADC, whose features are described in [9].

As shown in Fig. 3, the chip embeds two oscillators providing a 500 kHz and a 50 MHz clocks. The slow clock runs all the time and feeds the main control logic block. The latter governs the sampling frequency and generates the timing phases for the pixel array and associated stages, namely, the SFs, the sample and holds, and averaging stages. The control logic also governs the LED drivers and the amplifier. The fast clock is only used during the analog-to-digital conversion. In other words, power gating is used whenever the fast clock is not needed. Similarly to the fast clock, the power supply is also gated in order to optimize the chip power consumption. Fig. 4 depicts the drill down of the chip power consumption over time. The array circuit blocks are powered during the light integration and sampling, only. Once the samples are averaged, the amplifier and ADC are then powered to operate the conversion.

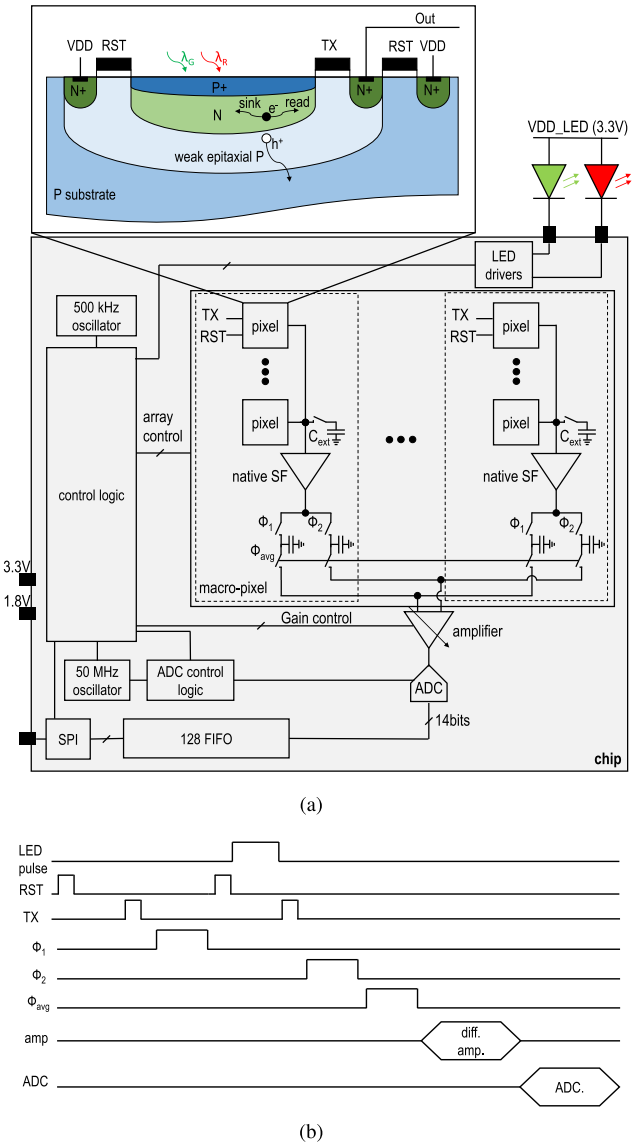

FIGURE 3. (a) A block diagram of the sensor depicting the macro-pixels array, the subtracting amplifier with ADC, and (b) corresponding timing diagram.

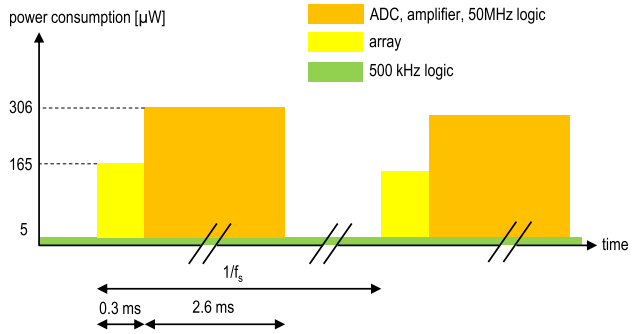

FIGURE 4. Sensor chip power consumption.

III. OPTICAL MODULE OPTIMIZATION

The optical module consists of the emitters (LEDs), the sensor chip, as shown in II, and an optical housing. The latter ensures a good optical coupling with the skin and at the

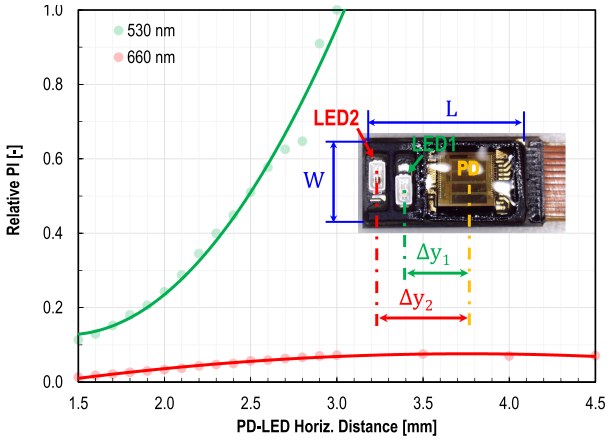

FIGURE 5. Simulated relations between relative PI and sensor-to-emitter (PD-LED) distance at 530 nm and 660 nm.

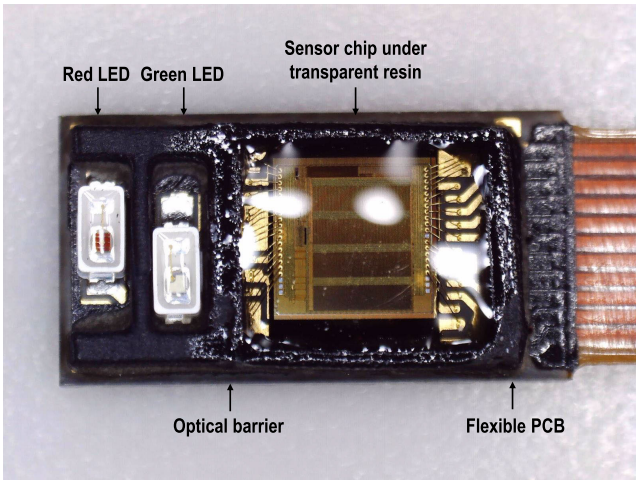

FIGURE 6. Photograph of the optimized optical module embedding LEDs, sensor chip covered by transparent resin, and optical barrier mounted on a flexible PCB.

same time a low direct light cross-talk between the sensor chip and the LEDs. It is obvious that the vertical distance between the skin and both the LEDs and the sensor must remain as short as possible to minimize the optical signal loss. However the horizontal distance separating the LEDs and the sensor chip requires a deeper thought. The optimization of the LED-sensor distance goes through a good understanding of the light-tissue interaction. In this work, we have reused the optical skin model presented in [11]. This model considers a seven layer structure and it has been proven sufficiently accurate to model primary effects of photon-skin interactions [12]–[14]. As shown in [11], TracePro® is used to simulate the non-pulsatile (DC) and pulsatile (AC) components of the optical signal. Fig. 5 shows the simulated relation between the relative PI (AC/DC) and the sensor-LED distance (δy), for green (530 nm) and red (600 nm) LEDs. The PI increases with δy for both wavelengths. However, the green light comes with better PI and features more sensitivity to δy, thanks to the intrinsic larger absorption.

Dim.	Typ. [mm]
D	19
W	7.9
t	3.8
f	1
b	1.22
2b/D	12.8%

FIGURE 7. Isometric and orthogonal views of the ring, including teardown of the electronic system.

The SNR is proportional to the PI and the number of photons received by the sensor [9]. Fig. 5 shows that the PI increases with the LED-sensor distance, but the number of received photons actually decreases. It is known that the optical decay follows an exponential trend. Hence the increase of PI with respect to δy is much weaker than the optical signal loss due to the LED-sensor distance. Hence, we have set δy to the minimum possible distance. Fig. 6 shows the resulting optical module. LED1 is an OSRAM CT DELSS1.12 with nominal wavelength at 530 nm, while LED2 is an OSRAM CH DELSS1.22 emitting at 660 nm. The wire bonding, the LEDs package and the minimum wall thickness set the minimum distance between the sensor and the LEDs, which is equal to 2.8 mm, center to center. Hence we have set the distance between the LED1 and the sensor (Δy_1) at its minimum of 2.8 mm. LED2 is placed at Δy_2 equal to 4 mm, which is the closest possible, i.e. placing it right next to LED1. The resulting module size ($W \cdot L \cdot H$) is $3.8 \cdot 7.1 \cdot 0.6\,\text{mm}^3$.

IV. THE RING SYSTEM DESIGN

A wearable ring was designed to embed the PPG module as in Fig. 6. Fig. 7 shows isometric and orthogonal views of the design, and a teardown image of the system, showing the PPG module connected to the microcontroller unit and a set of custom-shaped batteries. The ring diameter is chosen in the range 18 mm to 20 mm which has allowed to fit all the population in our study. The ergonomics of the ring is primarily dependent on the diameter (D) and secondly upon the thickness (t), width (w), internal filleting radius (f) and the position of the sensor (b). The thickness of the ring is optimized to provide inter-digits comfort and to preserve structural strength based on design guidelines for the chosen 3D printing process and material [15]. The combination of

TABLE 1. Sensor characteristics.

Device	PPG module	Application	Size	consumption
This work	Monolithic PPG sensor, true green and red LEDs	Heart beat monitoring	width: 7.9 mm thickness: 3.8 mm	2.5 mA without duty cycling
[16]	discrete PD, AFE, hyper red LEDs	Surgical pleth index	width: 10 mm thickness: 2 mm	3 mA
[2]	discrete PD, AFE, infrared LEDs	Sleep monitoring	width: 7.9 mm thickness: 2.55 mm	not reported

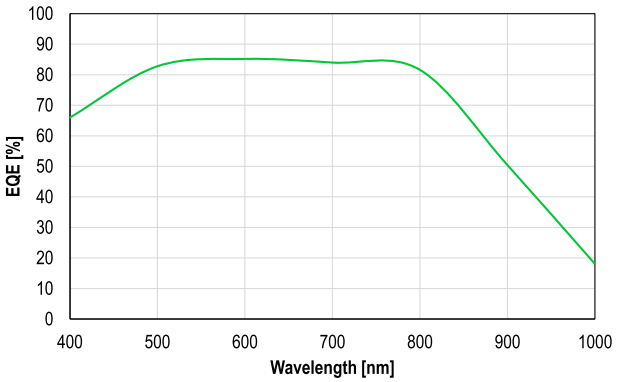

FIGURE 8. Measure EQE of two versions of the PPD based pixel dedicated for PPG with two weakly doped epitaxial layer depths. The measurement shows a better EQE for the pixels implemented in the presented work (18 μm epitaxial) particularly towards the NIR region.

w, f and b determines the mechanical strain of the skin. According to previous experimental observations, we have found an optimal point between the user's comfort and the PPG signal quality resulting from the pressure onto the skin at the area of optomechanical coupling of the sensor. In this study, a flat edge in the inner part of the ring is found to be at an optimal point when the ratio $2b/D$ is set at 12.8%. A functional prototype, Fig. 10, is 3D printed in stereolithography, because of its advantages such as being cost-effective and also featuring greater resolution for smaller features. A nylon-based material, EOS PA2200®, is selected because robust, flexible, stable for long periods of time and biocompatible under EN ISO 10993-1.

Table 1 compares the design of the presented ring with recent SOA. The presented ring offers a substantial advantage in terms of size and power consumption. Note that 2.5 mA is the current consumed of the whole ring when the Bluetooth-low-energy (BLE) and the micro-controller unit (MCU) are always on. For this study, we needed the ring to emit the data, via BLE, real time without any interruption to the computer. We expect this current consumption to be reduced by an order of magnitude, at least, if the data transmission is duty cycled.

V. OPTICAL MODULE MEASUREMENTS

Fig. 8 shows the measured effective QE (EQE) of the pixel. The proposed pixel features a weak P epitaxial depth

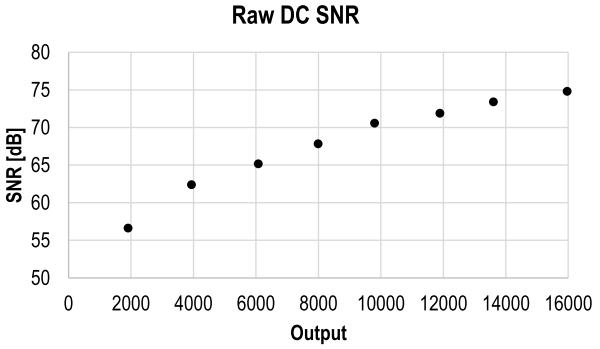

FIGURE 9. Measured SNR as a function of the sensor output obtained by operating the optical module, composed of the monolithic sensor and LED emitters, in loop-back mode. The SNR measurement takes into account all noise sources including shot noise, readout electronic noise, and the noise generated at the level of the LEDs.

of 12 μm. The proposed pixel demonstrates a clear advantage on the QE with respect to standard epitaxy pixels [8], especially in the NIR region. In fact, the EQE curve is close to 85% up to 800 nm.

Fig. 9 shows the SNR, measured on the sensor output raw data (without digital filtering), in loop-back mode, as a function of the output mean value. This measurement is obtained by exposing the module, composed of the sensor and LEDs, to a stable reflector. The emitting LEDs driving current is increased progressively resulting in an increase of the light intensity reflected on the monolithic sensor. Each point is obtained by measuring the noise and the mean values of the output, at a given LED driving current. In this way, this measurement of the SNR embeds not only the noise generated in the detection and readout process, but also the noise of the LED drivers and LED devices as well. The whole system can go up to 75 dB, without digital filtering. Since the PPG signal is anyway digitally filtered during the processing, the maximum SNR increases to 85 dB, after band limiting the signal between 0.1 Hz and 4 Hz by the means of a second order Butterworth filter. The presented optical module features similar performance with respect to the sensor presented in [11]. Indeed, the presented sensor features a larger pixel array but exploits the same amplifier and ADC design. The amplifier and ADC limit the performance in terms of SNR. Though, the larger pixel array enables collecting more signal photons compared to [11], which compensates for the more challenging body location.

Tab. 2 shows a summary of the main chip characteristics and performance metrics in comparison with recent state of the art. The introduced chip presents a monolithic solution that stands out in terms of silicon area, QE, power consumption and ambient light rejection, while embedding a 128 FIFO register, internal oscillators, and serial peripheral interface (SPI) protocol communication unit. These features are key for efficient integration in a wearable device, especially when paired with an optimal optical module design, as previously described.

FIGURE 10. Photograph of the ring device embedding the presented monolithic sensor and its optimized optical module.

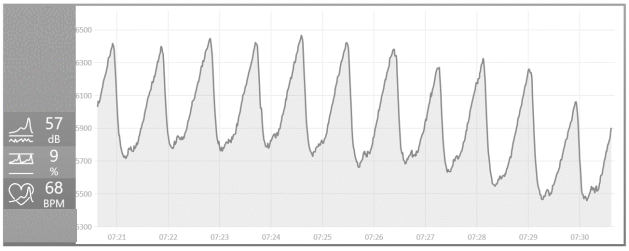

FIGURE 11. Example of a raw PPG recording obtained from the finger of a subject wearing the presented ring device.

In order to demonstrate the performance of the ring system in terms of PPG signal quality, Fig. 11 shows an example of a high SNR raw PPG signal recorded using the presented ring device. This PPG signal is recorded on the finger of a male subject wearing the ring as shown in Fig. 10. The recorded PPG signal features an SNR of 57 dB with a PI of 9%, while the sensor consumes less than 70 μA, including both the LEDs and the monolithic sensor chip.

The prototyped wearable ring led to further ex-vivo studies of the PPG signal at the finger location, the content of which is the object of the next session.

VI. RING SYSTEM VALIDATION FOR HEART BEAT MONITORING

In this section, the system-level performance of the presented ring device is evaluated, on several subjects, for heart beat monitoring.

A. IMPORTANCE OF ACCURATE BEAT DETECTION

Heart-rate variability (HRV), which is a physiological phenomenon that represents the change in the intervals of the consecutive heart-beats, is a very important index for the healthiness of the cardiovascular system. It is a measure of the cardiac activity that estimates the autonomous nervous system (ANS) balance [19]. As a matter of fact, HRV is closely associated with the overall physical fitness and the psychological well-being of an individual and it is used for stress and recovery analysis [19]. Since the outbreak of the COVID-19 pandemic the HRV data is becoming very crucial and is being heavily analyzed to study the effect of the COVID-19 on the mental health and the stress levels of individuals. HRV is also applied for sleep monitoring [20], and different types of arrhythmia detection [21], [22]. Therefore, it goes without saying that accurate, reliable, and continuous HRV monitoring is of utmost importance. An accurate HRV analysis, however, requires an efficient beat-to-beat heart rate detection [23], [24]. The classical method (the gold standard) of heart rate (HR) and HRV monitoring is using electrocardiography (ECG) devices. The drawback of the ECG recorders [25], [26] however is that they are highly uncomfortable and vulnerable to poor skin contact and dry skin conditions, which makes them unpleasant for long term recordings. As such, new solutions and methods that provide comfortable, unobtrusive, and inexpensive solutions are becoming highly attractive. Of these solutions and technologies, PPG is the most promising and favorable to provide low cost and agreeable alternative for HR and HRV monitoring.

TABLE 2. Sensor characteristics.

Parameter	This work	[17]	[18]
Monolithic (integrated photo-detector)	yes	no	yes
Process	180 nm CIS	180 nm	65 nm CIS
Voltage supply	3.3/1.8 V	3.3/1.2 V	1.8/1 V
Area	5.76 mm^2	7 mm^2	5.5 mm^2
Integrated FIFO and SPI/I2C	yes (128 words)	no	yes (64 words)
Max. sampling frequency	500 Hz	2048 Hz	20 Hz
Max. dynamic range	90 dB	119 dB	90 dB
ADC resolution	14 bit	14 bit	16 bit
Current consumption	60 μA @ 122 Hz including digital	74 μA @ 522 Hz excluding digital	24 μA @ 20 Hz including digital
Ambient light cancellation	64 dB @ 10 Hz with 20 dB/frequency decade decrease	not reported	direct 46 dB below 120 Hz

B. BEAT DETECTION USING THE RING

In what follows, we present a study that we have performed to examine the beat-to-beat detection accuracy of using the PPG signal recorded by the presented ring device. Seven male subjects with a mean age of 34.29 ± 5.28 years participate in the study. In total, 43 day and night recordings are performed with a total duration of 72.21 hours: 37.10 hours of *sleep* and

TABLE 3. The statistics of the reference RR intervals.

Number of RRI's	213072
Mean ± SD (ms)	1040 ± 170
pNN50 (%)	29.40
pNN20 (%)	71.13

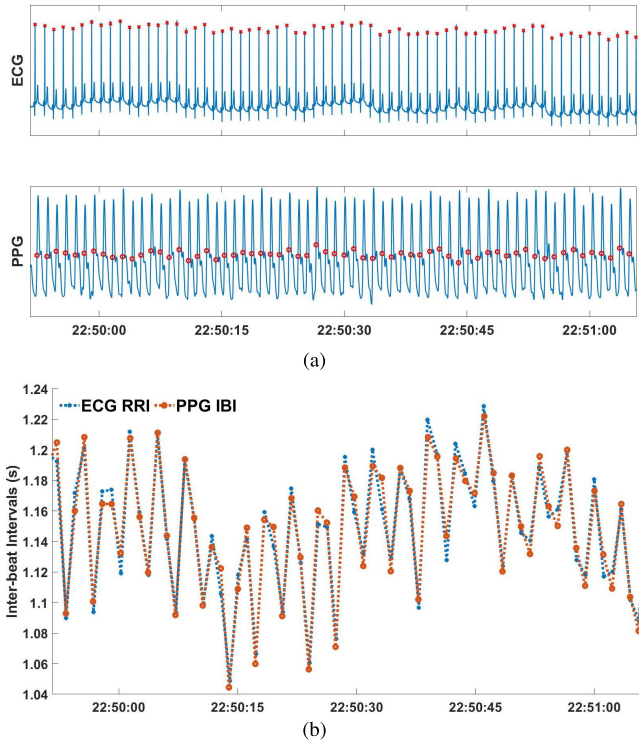

FIGURE 12. (a) A plot of ECG and PPG signals with R-peak and maximum up-slope detection (red labels), respectively. (b) Corresponding ECG-based RR intervals and PPG-based IBI's.

35.11 hours of *wake* recording. The participants are asked to wear the ring in the middle finger. The sampling frequency of the ring is set to 122 Hz and the driving current of the LED is set to 4.1 mA. For the reference ECG recordings, the Shimmer3 Consensys ECG development kit is used to monitor 4 ECG channels. The sampling frequency for the ECG recordings is set to 1024 Hz.

To extract the IBI values from the ring PPG signals, we have used the Senbiosys proprietary IBI detection software. On the other hand, to extract the RR intervals (RRI) from the ECG signals, the ConsensysPRO Software version 1.6.0 is used. In Fig. 12(a), we present plots of ECG and PPG recordings. The plots include (in red labels) the detection of R-peaks of the ECG signal and the detection of the maximum up-slopes of the PPG signal. These points are used to generate the ECG-based RR intervals and the PPG-based IBI values, depicted in Fig. 12(b).

Table 3 summarizes the statistics of the reference RRI values. The mean RRI value is 1.04±0.17 s, which means that on average the participants have HR values less than < 60 beats per minute. Moreover, the average HRV of the participants

TABLE 4. The beat detection performance.

Correctly Detected Beats	208539
Correct Beats (%)	97.87
Missed Beats (%)	2.13
Extra Beats (%)	1.40

TABLE 5. The performance of the IBI Estimation.

MAE (ms)	8.10
ME (ms)	0.24
RMSE (ms)	13.97
MAPE (%)	0.80

TABLE 6. The beat detection-estimation performance: wake vs sleep.

	Wake	*Sleep*
Correct Beats (%)	97.30	98.30
Missed Beats (%)	2.70	1.70
Extra Beats (%)	1.92	1.00
MAE (ms)	8.32	7.94
ME (ms)	0.79	−0.17
RMSE (ms)	15.96	12.48
MAPE (%)	0.80	0.81

can be considered to be fairly high with a pNN50 and pNN20[1] values of 29.40% and 71.13%, respectively.

C. PERFORMANCE EVALUATION

The performance of the IBI detection algorithm using the ring is summarized in Table 4. The results show that the percentage of the correctly detected beats is 97.87%. On the other hand, the percentage of the extra beats is only 1.40%. Table 5 summarizes the IBI estimation accuracy of the ring PPG with a mean absolute error (MAE) of 8.10 ms, a mean error (ME) of 0.24 ms, a root mean square error (RMSE) of 13.97 ms, and a mean absolute percentage error (MAPE) of 0.80%. As shown in Table 6, these beat detection and IBI estimation performance metrics improve for sleep/night recordings because of the absence of motion artifacts.

VII. DISCUSSION

The proposed monolithic PPG sensor design can trigger the advent of more and more smartrings. Indeed, on one hand, the finger PPG exhibits a fairly large PI with respect to other body locations, e.g. the wrist, leading to intrinsically better vitals extraction at lower power operations [1], but on the other hand, it can also suffer from some challenges. Among them, the motion-artifacts (MAs) and the PI reduction caused by hypothermia are among the toughest [27].

PPG spatial diversity, in essence the distribution of many PPG sensors around the sensing point, has proven to be

[1]pNN50 and pNN20 denote the percentage of the RR intervals with a successive difference exceeding 50 ms and 20 ms, respectively.

particularly effective in the smartwatches segment, to counterbalance the effect of MAs and lower perfusion [1]. The authors believe that the (smart) rings can also benefit from similar considerations, which will help to cope with the above-mentioned challenges. That said, unlike a smartwatch, the miniaturization constraints around a smart ring impose some limits, in terms of number of integrated PPG sensors, unless the PPG sensor itself becomes particularly miniaturized. The monolithic PPG sensor proposed in this work paves the way for such an approach thanks to the low power consumption and enhanced miniaturization.

VIII. CONCLUSION

This paper presents a cross disciplinary optimization of a wearable optical heart beat monitoring sensor integrated in a ring. The device embeds a monolithic optical sensor exploiting a CIS process. It encompasses dedicated pixels featuring an almost flat QE response on the whole visible range, while still exhibiting good NIR response. The dedicated pixels array is combined with low power design and CMOS integration to result in an ultra-low power and miniaturized sensor chip.

The advantages obtained thanks to the monolithic sensor integration are enhanced by an optimal optical module design, maximizing the PI of the PPG signal. The latter is optimized thanks to optical simulations emulating the LEDs, the optical module parameters of the human skin, and the sensor.

The performance is further enhanced by an ergonomic design of the ring allowing better diffusion of the light through the finger skin.

The ring system exhibits high SNR PPG signal (over 50 dB) while consuming less than 70 μA on both sensor and emitter side.

The system is validated for precise heart beat detection by comparison to a medical ECG device. The validation is performed on 7 subjects for a total of 72 hours of recording, distributed between wake and sleep time. 97.87% of the beats are correctly detected. The IBI estimation from these recordings exhibits an MAE of 8.10 ms.

The presented monolithic and low power solution paves the way for further miniaturization with advanced optical module packaging. The combination of further miniaturization and reduced power consumption eases the integration of a plurality of integrated independent PPG modules in a same ring device.

This proposed wearable optical heart beat monitoring system shows a promising potential for wellness and medical health monitoring thanks to the ease of use, non-evasiveness and long battery life. Further clinical studies shall be performed to bring this wearable technology to the medical heath monitoring market.

REFERENCES

[1] A. Caizzone, "An ultra low-noise micropower PPG sensor," Ph.D. dissertation, Dept. IMT, EPFL, Lausanne, Switzerland, 2020.
[2] (2021). *Ouraring*. [Online]. Available: https://ouraring.com
[3] E. Tur, M. Tur, H. I. Maibach, and R. H. Guy, "Basal perfusion of the cutaneous microcirculation: Measurements as a function of anatomic position," *J. Investigative Dermatol.*, vol. 81, no. 5, pp. 442–446, Nov. 1983. [Online]. Available: http://www.sciencedirect.com/science/article/pii/S0022202X15432312
[4] J. G. Webster, *Design Pulse Oximeters*. Bristol, PA, USA: Institute of Physics, 1997.
[5] A. Boukhayma, *Ultra Low Noise CMOS Image Sensors*. Cham, Switzerland: Springer, 2018.
[6] A. Boukhayma, A. Peizerat, and C. Enz, "A sub-0.5 electron read noise VGA image sensor in a standard CMOS process," *IEEE J. Solid State Circuits*, vol. 51, no. 9, pp. 2180–2191, Sep. 2016, doi: 10.1109/JSSC.2016.2579643.
[7] A. Boukhayma, A. Caizzone, and C. Enz, "Health monitoring device," U.S. Patent US20 200 205 680 A1, Jul. 21, 2017.
[8] A. Caizzone, A. Boukhayma, and C. Enz, "A 2.6μW monolithic CMOS photoplethysmographic sensor operating with 2μW LED power," in *IEEE Int. Solid-State Circuits Conf. (ISSCC) Dig. Tech. Papers*, Feb. 2019, pp. 290–291, doi: 10.1109/ISSCC.2019.8662404.
[9] A. Caizzone, A. Boukhayma, and C. Enz, "A 2.6 μW monolithic CMOS photoplethysmographic (PPG) sensor operating with 2 μW LED power for continuous health monitoring," *IEEE Trans. Biomed. Circuits Syst.*, vol. 13, no. 6, pp. 1243–1253, Dec. 2019, doi: 10.1109/TBCAS.2019.2944393.
[10] A. Boukhayma, A. Caizzone, and C. Enz, "An ultra-low power PPG and mm-resolution ToF PPD-based CMOS chip towards all-in-one photonic sensors," *IEEE Sensors J.*, vol. 19, no. 24, pp. 11866–118858, Sep. 2019.
[11] A. Boukhayma, A. Barison, S. Haddad, and A. Caizzone, "Earbud-embedded micro-power mm-sized optical sensor for accurate heart beat monitoring," *IEEE Sensors J.*, early access, Jul. 21, 2021, doi: 10.1109/JSEN.2021.3098861.
[12] V. V. Tuchin, S. Utz, and I. Yaroslavsky, "Tissue optics, light distribution, and spectroscopy," *Proc. SPIE Opt. Eng.*, vol. 33, no. 10, pp. 3178–3188, 1994.
[13] Y.-H. Kao, P. C.-P. Chao, and C.-L. Wey, "Design and validation of a new PPG module to acquire high-quality physiological signals for high-accuracy biomedical sensing," *IEEE J. Sel. Topics Quantum Electron.*, vol. 25, no. 1, Jan. 2019, Art. no. 69000210.
[14] Y. H. Kao, P. C. Chao, Y. Hung, and C. L. Wey, "A new reflective PPG LED-PD sensor module for cuffless blood pressure measurement at wrist artery," *Proc. IEEE Sensors*, Dec. 2017, pp. 1–3.
[15] B. De Zwart. (2014). *Additive Manufacturing Technologies*. [Online]. Available: https://www.3dhubs.com/
[16] C. Zhou, H. Wang, Y. Zhang, and X. Ye, "Study of a ring-type surgical pleth index monitoring system based on flexible PPG sensor," *IEEE Sensors J.*, vol. 21, no. 13, pp. 14360–14368, Jul. 2021.
[17] Q. Lin, J. Xu, S. Song, A. Breeschoten, M. Konijnenburg, C. Van Hoof, F. Tavernier, and N. Van Helleputte, "A 119dB dynamic range charge counting light-to-digital converter for wearable PPG/NIRS monitoring applications," *IEEE Trans. Biomed. Circuits Syst.*, vol. 14, no. 4, pp. 800–810, Aug. 2020.
[18] S. J. Jung, J. Ryu, W. Kim, S. Lee, J. Kim, and H. Park, "A 400-to-1000 nm 24μW monolithic PPG sensor with 0.3 A/W spectral responsivity for miniature wearables," in *IEEE Int. Solid-State Circuits Conf. (ISSCC) Dig. Tech. Papers*, vol. 64, Feb. 2021, pp. 1–3.
[19] J. Sztajzel, "Heart rate variability: A noninvasive electrocardiographic method to measure the autonomic nervous system," *Swiss Med. Wkly.*, vol. 134, nos. 35–36, pp. 514–522, 2004.
[20] T. Myllymäki, H. Rusko, H. Syväoja, T. Juuti, M.-L. Kinnunen, and H. Kyröläinen, "Effects of exercise intensity and duration on nocturnal heart rate variability and sleep quality," *Eur. J. Appl. Physiol.*, vol. 112, no. 3, pp. 801–809, Mar. 2012.
[21] S. Haddad, J. Harju, A. Tarniceriu, T. Halkola, J. Parak, I. Korhonen, A. Yli-Hankala, and A. Vehkaoja, "Ectopic beat detection from wrist optical signals for sinus rhythm and atrial fibrillation subjects," in *Proc. Medit. Conf. Med. Biol. Eng. Comput.*, Sep. 2019, pp. 150–158.
[22] A. Tarniceriu, V. Vuohelainen, S. Haddad, T. Halkola, J. Parak, J. Laurikka, and A. Vehkaoja, "Performance of wrist photoplethysmography in monitoring atrial fibrillation in post cardiac surgery patients," in *Proc. Comput. Cardiol. (CinC)*, Sep. 2019, pp. 1–4.
[23] U. R. Acharya, K. P. Joseph, N. Kannathal, C. M. Lim, and J. S. Suri, "Heart rate variability: A review," *Med. Biol. Eng. Comput.*, vol. 44, no. 12, pp. 1031–1051, Dec. 2006.

[24] M. Malik, "Heart rate variability," *Eur. Heart J. Trans. Neural Netw.*, vol. 17, pp. 354–381, 1996.
[25] L. C. M. Vanderlei, R. A. Silva, C. M. Pastre, F. M. Azevedo, and M. F. Godoy, "Comparison of the polar S810i monitor and the ECG for the analysis of heart rate variability in the time and frequency domains," *Brazilian J. Med. Biol. Res.*, vol. 41, no. 10, pp. 854–859, Sep. 2008.
[26] L. Porto and L. Junqueira, "Comparison of time-domain short-term heart interval variability analysis using a wrist-worn heart rate monitor and the conventional electrocardiogram," in *Pacing Clin. Electrophysiol.*, vol. 32, Jan. 2009, pp. 43–51.
[27] K. Budidha and P. A. Kyriacou, "Investigation of photoplethysmography and arterial blood oxygen saturation from the ear-canal and the finger under conditions of artificially induced hypothermia," in *Proc. 37th Annu. Int. Conf. IEEE Eng. Med. Biol. Soc. (EMBC)*, Aug. 2015, pp. 7954–7957.

ASSIM BOUKHAYMA was born in Rabat, Morocco, in February 1988. He received the Ph.D. degree from the École Polytechnique Fédérale de Lausanne (EPFL), Lausanne, Switzerland, on the subject of ultra-low noise CMOS image sensors. He received the Springer thesis award in recognition for his Ph.D. outstanding Research. He is currently the Founder and the Chief Scientific Officer at Senbiosys SA, Neuchâtel, Switzerland, and a Scientific Advisor for EPFL. From 2012 to 2016, he worked at Commissariat a l'Energie Atomique (CEA-LETI), Grenoble, France, in the frame of his Ph.D. research. From 2016 to 2019, he worked as a Research Team Leader at the Integrated Circuits Laboratory, EPFL.

ANTHONY BARISON received the M.Sc. degree in biomedical engineering from the Swiss Federal Institute of Technology (ETH) Zürich, Zürich, Switzerland, in 2019.

He is currently a System Engineer at Senbiosys SA, Neuchâtel, Switzerland. His research interests include skin optics and opto-mechanical integration of photoplethysmography systems in wearable devices. He received the 2013 IEEE U.K. and RI Communication Chapter Prize in merit of his work on mm-wave steerable antennas at the University of Essex, Colchester, U.K.

SERJ HADDAD received the B.E. and M.Sc. degrees in computer engineering from Lebanese American University (LAU), in 2010 and 2012, respectively, and the Ph.D. degree in computer and communication sciences from the École Polytechnique Fédérale de Lausanne (EPFL), in 2017. He is currently a Research Engineer at Senbiosys SA, working on developing algorithms for optical signals. His research interests include biomedical signal processing, random matrices, free space optics, and network information theory.

ANTONINO CAIZZONE (Member, IEEE) was born in Milazzo, Italy, in March 1991. He received the Ph.D. degree from the École Polytechnique Fédérale de Lausanne (EPFL), under the supervision of Prof. Enz and Dr. Boukhayma, on the subject of ultra-low noise and low power sensors for healthcare.

He is currently the Founder and the Chief Technology Officer at Senbiosys SA, Neuchâtel, Switzerland. From 2012 to 2013, he worked at STMicroelectronics, Italy, as an Intern, on the design of analog electronics on plastic substrate. In 2014, he worked at Georgia Tech, USA, as a Visiting Researcher on the subject of energy harvesters.